RSC Advances

ROYAL SOCIETY OF CHEMISTRY

www.rsc.org/advances

Journal Name

ARTICLE

Ultra-thin V_2O_5 Nanosheets Based Humidity Sensor, Photodetector and Its Enhanced Field Emission Properties

Received 00th January 20xx,
Accepted 00th January 20xx

DOI: 10.1039/x0xx00000x

www.rsc.org/

Mahendra S. Pawar[a], Prashant K. Bankar[b], Mahendra A. More[b] and Dattatray J. Late[a,*]*

We report synthesis of V_2O_5 nanosheets by simple hydrothermal method. The as synthesized V_2O_5 nanosheets we characterized by using Raman Spectroscopy, Field Emission Scanning Electron Microscopy (FESEM), Transmission Electron Microscopy (TEM) and UV-Vis Spectroscopy. The humidity sensing behaviors were investigated in the range of 11-97% of relative humidity (RH) at room temperature. The maximum sensitivity of 45.3%, response time of ~ 4 min. and recovery time of ~ 5 min. were observed for the V_2O_5 nanosheets based sensor. We also demonstrated the V_2O_5 nanosheets as Ultra-Violet photodetector with sensing response time of ~ 65 s and recovery time of ~ 75 s with maximum photoresponsivity of ~ 6.2% were observed. Further, We have also carried out field emission (FE) investigations of V_2O_5 nanosheets under planer "Diode" assembly in ultrahigh vacuum (UHV) chamber at a base pressure of ~1 x 10^{-8} mbar. The turn on field required to draw field emission current density of 1 μA/cm^2 and 10 μA/cm^2 is found to be 1.15 V/μm and 1.72 V/μm respectively. We achieved maximum field emission current density of 1.532 mA/cm^2 at an applied electric field of 3.2 V/μm. The field enhancement factor calculated from the slope of Fowler – Northeim (F-N) plot is found to be 8530 and 3530 at low field and high field region respectively. Our results open up several avenues and key success towards the utilization of V_2O_5 nanosheets and other metal oxide nanosheets for various nanoelectronics device applications including sensors, photodetector and flat panel displays.

Introduction

Since the invention of graphene, atomically thin two dimensional (2D) materials have attracted enormous attention due to their potential applications in next generation nano-electronics and optoelectronics device[1,2]. The first 2D layered materials isolated were graphene followed by several inorganic layered such as MoS_2, WS_2, $MoSe_2$, WSe_2, Black Phosphorous[58] etc. and metal oxides materials such as MoO_3, WO_3, MnO_2 were invented for various applications including humidity sensor[3-8], photodetector[9-23], transistor[24], gas sensor[25,26], solar cell[43-46], supercapacitor[47-50], catalyst for water splitting[51,52]etc. Humidity sensors have been developed to measure and monitor the environmental humidity that plays an important role in the agriculture, food as well as medical industry along with human activities[27]. The layered V_2O_5 is most stable oxide as compared with other oxides of vanadium. The 2D form of V_2O_5 has high surface to volume ratio and high oxidation state at nanoscale geometry. Recently nanostructure V_2O_5 has been used in various application including field emission[29-30, 59-62],

supercapacitor[31-34], Li ion battery[35], transistor[36], Photodetector[37] etc. A variety of methods of synthesis of V_2O_5 nanostructures have been reported till date including hydrothermal[28, 53,54], electrospinning[55,56], polycondensation method[57]. Among them, hydrothermal method is widely used for the synthesis of V_2O_5nanostructures due to low cost, fast reaction time, well controlled morphology and highly pure product. In hydrothermal method, the morphology of the materials can be tuned by the hydrothermal temperatures which can be kept slightly below the melting point of the reactants and also by varying the concentration of solvents used. The nanostructure V_2O_5 possesses direct bandgap of 2.2 eV to 2.7 eV in the visible light region which inspires to investigate the optoelectronic properties such as photodetection[37], optical waveguide[39] and high speed photoelectric switchs[38].

In this paper, we report V_2O_5 nanosheets based humidity sensor with superior performance with fast response and recovery time along with the high sensitivity. We also demonstrated the photodetector based on V_2O_5 nanosheet with fast response time ~65 sec and recovery time of ~75 sec to UV light. We have also done the field emission measurement for V_2O_5 nanosheets. We achieved turn on field to be 1.15 V/µm and maximum current density of ~1.532 mA/cm^2 at an applied field of 3.2 V/µm with high field enhancement factor of ~8580 shows applications in flat panel displays, electron emitter etc.

Experimental

Materials

Commercially available Vanadium (V) Oxide (Sigma-Aldrich, 99.99%) and Dodecylamine (Sigma-Aldrich, ≥ 99%) were used for the synthesis of V_2O_5 nanosheets. The required salts for humidity sensing were purchased from the Thomas Baker chemicals Pvt. Ltd. Mumbai (India).

Synthesis Method

The V_2O_5 nanosheets were synthesized using simple hydrothermal method for that V_2O_5 (15 mM) and Dodecylamine (7.5 mM) were mixed with 5 ml of ethanol stirred for 2hr. To this mixture 15 ml of DI water was added and stirring was continued for further 48 hrs, then the mixture was transferred into the 50 ml Teflon lined stainless steel autoclave and placed in muffle furnace at 180^{0}C for 7 days. T obtained black precipitate was finally washed with ethanol f several times followed by centrifugation and the precipitate was th dried in a vacuum furnace at 80^{0}C for 12 hrs.

Material Characterizations

The samples were characterized by using Raman Spectroscopy with Horiba JY Lab HR 800 instrument using Ar laser with wavelength of 632.5nm operated in the back scattering geometry with synapse CCD detector. The surface morphology were investigated by using FESEM with HITACHI S-4800 instrument and the TEM images were captured using FEI TECNAI G2-20 (TWIN, The Netherlands) instrument operating at 200 KV. A UV-Vis spectrum was recorded using Shimadzu (UV-3600) Plus UV-Vis-NIR Spectrophotometer in the wavelength range 200-1300 nm.

Sensor Device Fabrication

The humidity sensor as well as photodetector devices were fabricated on an ITO (Tin doped Indium Oxide) substrate by making scratch at the centre on the conducting surface with the help of glass cutter with separation between source and drain was ~ 1 0 µm. The contacts were then made using silver paint. For devic preparation the as synthesized V_2O_5 nanosheets powder were

dispersed into the ethanol and then ultrasonicated for 10 min, and subsequently drop casted between the source and drain. The devices were subsequently annealed in vacuum furnace at 200^0C to improve the contact resistance.

Humidity Sensing

All the electrical measurements were carried out using Keithley 2612A system source meter which was attached to a computer through GPIB 488A interface. The response of the device as a function of RH was performed by introducing the device inside the closed RH levels. The relative humidity levels were obtained by keeping the saturated salts of LiCl, $MgCl_2$, K_2CO_3, NaBr, KI, NaCl, KCl and K_2SO_4 in a closed vessel.

Photodetector

To investigate the photo detection property we used HAMAMATSU (Model name: L9566-01A-02) UV light source. All the measurements were carried out at room temperature and in identical conditions.

Field Emission

All the field emission (FE) measurements were carried out at room temperature in the planer "Diode" assembly in an all metal ultrahigh vacuum (UHV) chamber at a base pressure of ~1 x 10^{-8} mbar. A typical 'diode' configuration consists of a phosphor coated semitransparent screen as an anode. In order to investigate the FE properties, V_2O_5 nanosheets were sprinkled onto a piece of carbon tape (0.3 cm × 0.3 cm). Such V_2O_5 sprinkled carbon tape was pasted onto a copper rod holder (diameter ~ 50 mm), which acted as a cathode. The FE measurements were carried out at fixed cathode–anode separation of ~ 2 mm. The emission current density - applied field and current – time measurements were carried out using Keithley (6514) electrometer by sweeping DC voltage applied to cathode with a step of 40V (0 - 40 KV, Spellman, U.S.). The field emission current stability was recorded at preset current value of 1 μA using computer controlled data acquisition system.

Results and Discussion

Characterization analysis

Figure 1 (a) shows the typical side view of the single-layer V_2O_5 nanosheet and figure 1(b) shows the top view. In figure 1(c) we show the typical experimental set-up used for the UV photo detection. The Raman Spectrum for V_2O_5 nanosheets as well as for the bulk V_2O_5material were shown in Figure 2.The observed Raman spectra for V_2O_5 nanosheets matches well with that reported previously in the literature[28,41-42]. The Raman shift corresponds to different modes of vibrations are 143, 194, 286, 408, 525, 693 and 993 cm^{-1}.The Raman spectra are found to be slightly down shifted for V_2O_5 nanosheets as compared to the V_2O_5bulk material due to decrease in interlayer bonding. The Raman mode 993 and 693 cm^{-1} corresponds to the stretching modes of V=O terminal oxygen and V_2-O i.e. doubly coordinated oxygen bonds respectively which is triply coordinated oxygen bonds. The Raman mode observed at 525 cm^{-1} corresponds to the stretching mode of V_3-O i.e. triply coordinated oxygen bonds. The bending vibration of the V=O bonds arises for the 408 and 286 cm^{-1} modes. The Raman mode frequency 143 and 194 cm^{-1} corresponds to the external VO_5 – VO_5 modes. Figure 3(a-d) shows the typical FESEM images of the as synthesized V_2O_5 nanosheets which indicates that the high yield of nanosheets synthesized by using hydrothermal method. Typical FESEM images show V_2O_5 nanosheets with lateral dimensions in few tens of micrometers. Figure 4(a-d) shows the TEM images of V_2O_5 nanosheets and figure 4(e) shows the HRTEM image taken from the

V_2O_5 nanosheet which depicts the interplanar distance between the two plane is ~ 0.35 nm, which corresponds to (202) plane of the V_2O_5. Figure 4(f) shows the corresponding selected area electron diffraction pattern which shows crystalline nature of the V_2O_5 nanosheets.

Optical Properties

To investigate the optical properties of the V_2O_5 nanosheets, we recorded the UV-Vis Spectrum as shown in figure 5. The spectrum represents the major absorption bands for V_2O_5 nanosheets ~ 410 nm. Our UV-Vis spectrum matches well with the reported spectrum of V_2O_5 nanosheets in the literature[64].

Humidity Sensor

The V_2O_5 nanosheets synthesized by using hydrothermal method were used to further investigate the humidity sensing performance. The humidity sensing properties were investigated by fabricating the two probe device and then introducing to different relative humidity (RH) conditions, which were attained by using saturated salt solutions. It is noted that all the humidity measurements were carried out at room temperature. Figure 6(a) shows the current – voltage (I-V) characteristics of V_2O_5 sensor device in different RH levels. It is clear from the (I-V) that the current decreases with the increase in relative humidity value. Figure 6(b) shows the resistance Vs relative humidity plot for the V_2O_5 nanosheets based sensor device. The obtained (I-V) curve represents that the resistance increases with the increasing relative humidity (RH) levels. The sensitivity as a function of relative humidity plot was also shown in figure 6(c). The sensitivity of the device depends on the number of H_2O molecules adsorbed on the V_2O_5 nanosheets. We observed the positive sensitivity for the presented V_2O_5nanosheets based sensor with increased RH levels. The sensitivity for V_2O_5 nanosheets sensor is defined as $S = \frac{R_H}{R_A} - 1$, where R_H and R_A is the resistances of the device to the humidity and in air respectively. The positive sensitivity implies that the H_2O molecules present in the saturated salts acts as an electron acceptor which results in the p-type doping. The water molecules present in the saturated salts adsorbed on the surface of V_2O_5 nanosheets which shifts the Fermi level closer to the valence band edge. The maximum sensitivity for the presented V_2O_5nanosheets sensor device was calculated to be 45.3%.The response and recovery time for the V_2O_5 nanosheets based sensor device were shown in figure 6(d). The cycles of 11.3% and 97.3% RH were used to record the response and recovery time. The current – time (I-t) measurements were carried out for several cycles to check the reproducibility in the response and recovery time. The response and recovery time for the V_2O_5 nanosheets sensor were found to be 4 min. and 5 min. respectively. The long recovery time may be due to slow desorption process of H_2O molecules from the V_2O_5 nanosheets and the faster response is due to hydrophilic surface of the V_2O_5 nanosheets results into immediate adsorption of H_2O molecules on the surface of nanosheets[65]. Another reason is due to the thickness of V_2O_5 nanosheets layer, thicker the sheet recovery will be more because desorption of H_2O molecules is difficult in the thick sheets so recovery time will be less in case of thin sheets. The response of the sensors device is based on strong adsorption / desorption of analyte molecules at room temperature along with traps or impurities at V_2O_5 and underlying substrate interface. The slow response is related to the activation energy of binding gas molecules to the V_2O_5 nanosheets. The response can be faster with light irradiation, manifested by the slope change during response[3]. The response rate can be improved by applying light irradiation, / increasing operating temperature. The traps at V_2O_5/ substrate

interface are also possibly responsible for the slow recovery. However, we suspect that if this is the dominate factor, we should see recovery / response much slower in thick layer sample as compared with thin layer sample, since our device requires longer time for the gas molecules to diffuse into interface.

UV Photodetector

The V_2O_5 nanosheets synthesized by using hydrothermal method were also used for UV light photo detection. Figure 7(a) shows the (I-V) characteristics of the V_2O_5 nanosheets sensor device with power density of UV light used upto 200 mW/cm^2. We observed that the current increases with the increasing power density of UV light. Photocurrent as a function of power density plot was shown in Figure 7(b) which indicates that the Photocurrent increases with the increasing power density. Photocurrent is the difference in the current recorded in the light illumination condition and the current recorded in the dark condition. Figure 7(c) shows the photoresponsivity Vs power density plot. The photoresponsivity is defined as the ratio of photocurrent to power density. We observed that the photoresponsivity increases with the increasing power density. We observed the maximum photoresponsivity of ~ 6.2 μAcm^2/W for 200 mW/cm^2 power density. The photocurrent response of the V_2O_5 nanosheets photodetector is shown in Figure 7(d), which is measured under the 365 nm light illumination with on and off cycles at applied bias voltage of 1V. The Response and recovery time with the V_2O_5 nanosheets based sensor is found to be ~ 65 sec and ~ 75 sec respectively.

Field Emission

As synthesized V_2O_5 nanosheets were further used to investigate the field emission properties. Figure 8(a) depicts the field emission current density versus an applied electric field (J-E) characteristics of V_2O_5 nanosheets. It is noted that the current density exponentially increases with an elevated applied electric field, indicating that the emission is as per the Fowler–Nordheim (F–N) theory[63]. It demonstrate a turn-on and threshold field defined as, field require to draw an emission current density of ~ 1 μA/cm^2 and ~ 10 μA/cm^2, respectively is found to be 1.15 and 1.72 V/μm. Interestingly, an emission current density of 1.532 mA/cm^2 is achieved at an applied field of 3.2 V/μm. The results suggest that the observed value of turn-on and threshold field is much lower than the earlier reported values for different V_2O_5 nanostructures. The comparison of FE properties between the as-synthesized product and various V_2O_5 nanostructures is shown in table 1. As noticed from the SEM image, most of the V_2O_5 nanosheets are randomly oriented, it could be expected that some of them will protrude outside the substrate surface, which act as potential emitting sites. The dependence of field electron emission current density over applied field (J-E) is further characterized by modified Fowler-Nordheim (F-N) theory[63] using the following equation,

$$J = \lambda_M a\phi^{-1}E^2\beta^2 \exp\left(-\frac{b\phi^{\frac{3}{2}}}{\beta E}v_F\right) \quad \text{..... (1)}$$

Where, J is the emission current density, E is the applied average electric field, a and b are constants, typically 1.54 × 10^{-6} A eV V^{-2} and 6.83 eV$^{-3/2}$ Vnm^{-1}, respectively, ϕ is the work function of the emitter material, λ_M be the macroscopic pre-exponential correction factor, vF is value of the principal Schottky–Nordheim barrier function (a correction factor), and β is the field enhancement factor. In the present investigations, the applied electric field (E) is defined as E=V/d, where V is the applied voltage, and d is the separation between anode and cathode (~ 2 mm). Furthermore, the emission current density (J) is estimated as J = I/A, where, I is the

emission current and A is the total area of the emitter. The J-E characteristic is further analyzed by plotting a graph of ln (J/E^2) versus (1/E), known as a Fowler-Nordheim (F-N) plot. The corresponding F-N plot is shown in Figure 8(b). In the present study, the F-N plot is found to be nonlinear and such F-N plots have been reported for many semiconducting nanomaterials. The nonlinearity in the F-N plot can be resolved into two linear sections with distinct slopes in the high-field and low-field regions (See Fig.8(b)). The field enhancement factors (β) are calculated from the slope of the low-field and the high-field regions of the F-N plot, using the following equation (2),

$$\beta = -\frac{6.8\times10^3\times\phi^{\frac{3}{2}}}{slope} \qquad \ldots\ldots\ldots\ldots (2)$$

The field enhancement factor for low field and high field regions are found to be 8580 and 3538 respectively. These calculated values of may be overestimates due to the limitation of the F-N equation. For the application purpose in field emission based devices, emission current stability deceives an important parameter. The emission current and time (I-t) plot recorded at a base pressure of ~1 X 10^{-8} mbar is shown in Figure 8(c). The average emission current is seen to remain stable at pre-set value of ~1 μA over three and half hour. The emission current is seen to be stable over the duration of measurement and characterized by fluctuation in the form of "spike". The appearance of the ''spikes'' in the emission current is attributed to the adsorption, desorption, and migration of the residual gas molecules on the emitter surface. The striking feature of the observed field emission behavior is that the average emission current remains nearly constant over the entire duration and shows no signs of degradation. This is very important feature particularly from the practical application of the emitter material as an electron source. Typical FE image, captured at emission current of ~50μA/cm^2, is shown in Figure8(d). The image show a number of tiny spots, corresponding to the emission from the most protruding edges of V_2O_5 nanosheets. The temporal changes in the intensity of these spots are observed to be commensurate with the emission current fluctuation, depicted in the I–t plot.

Conclusion

In conclusion, we report the simple synthesis of V_2O_5 nanosheets by one step hydrothermal method. The as synthesized V_2O_5 nanosheets were characterized using Raman Spectroscopy, FESEM, TEM and UV-Vis Spectroscopy. The humidity sensing performances were carried out over a range of 11-97% relative humidity at room temperature. The maximum sensitivity of ~ 45.3% and response time of ~ 4 min. and recovery time ~ 5 min. were observed for the V_2O_5 nanosheets sensor. Further, the as synthesized V_2O_5 nanosheets also shows good performance towards UV photodetector with response time of ~ 65 sec and recovery time of ~75 sec with maximum photoresponsivity of ~ 6.2 %. The field emission properties were studied in planer "Diode" assembly at base pressure of ~ 1x10^{-8} mbar. The turn on field required to draw an emission current density of 1 μA/cm^2 and 10 μA/cm^2 is found to be 1.15 and 1.72 V/μm respectively which is very less as compared to previous reports for different V_2O_5 nanostructures. We achieved emission current density of 1.532 mA/cm^2 at an applied field of 3.2 V/μm and also high field enhancement factor 8580 and 3538 for low field and high field region. Our results open up several avenues and key success towards the utilization of other oxide nanosheet materials with layered structure for various energy harvesting, optoelectronics and nanoelectronics device applications including sensors, photodetector, flat panel displays, electron source and transistor.

Acknowledgements

Dr. D. J. Late would like to thank Prof. C. N. R. Rao (FRS), JNCASR and ICMS Bangalore (India) for encouragement, support and the experimental facilities. The research work was supported by Department of Science and Technology (Government of India) under Ramanujan Fellowship to Dr. D. J. Late (Grant No. SR/S2/RJN-130/2012), NCL-MLP project grant 028626, DST-SERB Fast-track Young scientist project Grant No. SB/FT/CS-116/2013, Broad of Research in Nuclear Sciences (BRNS) Grant No. 34/14/20/2015 (Government of India) and the partial support by INUP IITB project sponsored by DeitY, MCIT, Government of India.

Notes and References

[1] Q. H. Wang, K. Kalantar-Zadeh, A. Kis, J. N. Coleman and M. S. Strano, *Nat. Nanotechnol.*, 2012, **7**, 699–712.

[2] (a) M. Buscema, J. O. Island, D. J. Groenendijk, S. I. Blanter, G. A. Steele, H. S. J. van der Zant and A. Castellanos-Gomez, *Chem. Soc. Rev.*, 2015, **44**, 3691–3718. (b) D. J. Late, Advanced Device Materials 2015, **1**, 52-58.

[3] Z. Li, H. Zhang, W. Zheng, W. Wang, H. Huang, C. Wang, A. G. MacDiarmid and Y. Wei, *J. Am. Chem. Soc.*, 2008, **130**, 5036–5037.

[4] H. Bi, K. Yin, X. Xie, J. Ji, S. Wan, L. Sun, M. Terrones and M. S. Dresselhaus, *Sci. Rep.*, 2013, **3**, 2714-2720.

[5] J. Chu, X. Peng, P. Feng, Y. Sheng and J. Zhang, *Sensors Actuators, B Chem.*, 2013, **178**, 508–513.

[6] M. V. Kulkarni, S. K. Apte, S. D. Naik, J. D. Ambekar and B. B. Kale, *Sensors Actuators, B Chem.*, 2013, **178**, 140–143.

[7] P. G. Su and Z.-M. Lu, *Sensors Actuators B Chem.*, 2015, **211**, 157–163.

[8] Q. Y. Tang, Y. C. Chan and K. Zhang, *Sensors Actuators, B Chem.*, 2011, **152**, 99–106.

[9] F. Xia, T. Mueller, Y.-M. Lin, A. Valdes-Garcia and P. Avouris, *Nat. Nanotechnol.*, 2009, **4**, 839–843.

[10] S. H. Yu, Y. Lee, S. K. Jang, J. Kang, J. Jeon, C. Lee, J. Y. Lee, H. Kim, E. Hwang, S. Lee and J. H. Cho, *ACS Nano*, 2014,**8**, 8285–8291.

[11] Y. Chang, O. W. Zhang, O. Y. Zhu, Y. Han, J. Pu, J. Chang and W. Hsu, *ACS Nano,*2014,**8**, 8582–8590.

[12] N. Huo, S. Yang, Z. Wei, S.-S. Li, J.-B. Xia and J. Li, *Sci. Rep.*, 2014, **4**, 5209-5217.

[13] (a) D. J. Late, P. A. Shaikh, R. Khare, R. V. Kashid, M. Chaudhary, M. A. More and S. B. Ogale, *ACSAppl. Mater. Interfaces*, 2014, **6**, 15881-15888. (b) D. J. Late, B. Liu, H. S. S. R. Matte, V. P. Dravid, C. N. R. Rao, ACS Nano 2012, **6**, 5635-5641 (c) D. J. Late, B. Liu, H. S. S. Matte, C. N. R. Rao, V.P. Dravid, Adv. Funct. Mater. 2012, **22**, 1894-1905. (d) M Thripuranthaka, D. J. Late, ACS Applied Materials Interfaces 2014, **6**, 1158–1163; (e) D. J. Late, S. N. Shirodkar, U. V. Waghmare, V. P. Dravid, C. N. R. Rao, ChemPhysChem 2014, **15**, 1592–1598; (f) M. Thripuranthaka, R.V. Kashid, C. S. Rout, D.J. Late, Appl. Phys. Lett. 2014, **104**, 081911. (g) D. Chakravarty, D. J. Late, European Journal of Inorganic Chemistry 2015 (11), 1973–1980.

[14] S. Lei, L. Ge, Z. Liu, S. Najmaei, G. Shi, G. You, J. Lou, R. Vajtai and P. M. Ajayan, *Nano Lett.*, 2013, **13**, 2777–2781.

[15] S. Lei, A. Sobhani, F. Wen, A. George, Q. Wang, Y. Huang, P. Dong, B. Li, S. Najmaei, J. Bellah, G. Gupta, A. D.

Mohite, L. Ge, J. Lou, N. J. Halas, R. Vajtai and P. Ajayan, *Adv. Mater.*, 2014, **26**, 7666–7672.

[16] O. Lopez-Sanchez, D. Lembke, M. Kayci, A. Radenovic and A. Kis, *Nat. Nanotechnol.*, 2013, **8**, 497–501.

[17] J. Wang, M. S. Gudiksen, X. Duan, Y. Cui and C. M. Lieber, *Science*, 2001, **293**, 1455–1457.

[18] J. Xia, X. Huang, L.-Z. Liu, M. Wang, L. Wang, B. Huang, D.-D. Zhu, J.-J. Li, C.-Z. Gu and X.-M. Meng, *Nanoscale*, 2014, **6**, 8949–8955.

[19] C. Zhang, S. Wang, L. Yang, Y. Liu, T. Xu, Z. Ning, A. Zak, Z. Zhang, R. Tenne and Q. Chen, *Appl. Phys. Lett.*, 2012, **100**, 243101-243105.

[20] K. Liu, M. Sakurai and M. Aono, *Sensors*, 2010, **10**, 8604–8634.

[21] L. Hu, J. Yan, M. Liao, L. Wu and X. Fang, *Small*, 2011, **7**, 1012–1017.

[22] D.-Y. Guo, C.-X. Shan, S.-N. Qu and D.-Z. Shen, *Sci. Rep.*, 2014, **4**, 7469-7474.

[23] K. Deng, H. Lu, Z. Shi, Q. Liu and L. Li, *ACS Appl. Mater. Interfaces*, 2013, **5**, 7845–7851.

[24] D. J. Late, B. Liu, J. Luo, A. Yan, H. S. S. R. Matte, M. Grayson, C. N. R. Rao and V. P. Dravid, *Adv. Mater.*, 2012, **24**, 3549–3554.

[25] V. Galstyan, E. Comini, G. Faglia and G. Sberveglieri, *Sensors (Basel).*, 2013, **13**, 14813–38.

[26] (a) D. J. Late, Y. K. Huang, B. Liu, J. Acharya, S. N. Shirodkar, J. Luo, A. Yan, D. Charles, U. V. Waghmare, V. P. Dravid and C. N. R. Rao, *ACS Nano*, 2013, **7**, 4879–4891. (b) DJ Late, T Doneux, M Bougouma, App. Phys. Lett. 2014, **105**, 233103. (c) P. K. Kannan, D. J. Late, H. Morgan, C. S. Rout, Nanoscale 2015, **7**, 13293-13312 (d) D. J. Late, C. S. Rout, D. Chakravarty, S. Ratha, Canadian Chemical Transactions 2015, 3, 118-157.

[27] G. Li, S. Pang, L. Jiang, Z. Guo and Z. Zhang, *J. Phys. Chem. B*, 2006, **110**, 9383–9386.

[28] M. Niederberger, H. J. Muhr, F. Krumeich, F. Bieri, D. Günther and R. Nesper, *Chem. Mater.*, 2000, **12**, 1995–2000.

[29] M. C. Wu and C. S. Lee, *J. Solid State Chem.*, 2009, **182**, 2285–2289.

[30] W. Chen, C. Zhou, L. Mai, Y. Liu, Y. Qi and Y. Dai,*J. Phys. Chem. C.* 2008,**112**, 2262–2265.

[31] L. Cao, J. Zhu, Y. Li, P. Xiao, Y. Zhang, S. Zhang and S. Yang, *J. Mater. Chem. A*, 2014, **2**, 13136-13142.

[32] D. Kim, J. Yun, G. Lee and J. S. Ha, *Nanoscale*, 2014, **6**, 12034–12041.

[33] S. Myung, M. Lee, G. T. Kim, J. S. Ha and S. Hong, *Adv. Mater.*, 2005, **17**, 2361–2364.

[34] Y. Wang and G. Cao, *Chem. Mater.*, 2006, **18**, 2787–2804.

[35] L. Mai, F. Dong, X. Xu, Y. Luo, Q. An, Y. Zhao, J. Pan and J. Yang,*Nano lett.,*2013,**13**, 740-745.

[36] G. T. Kim, J. Muster, V. Krstic, J. G. Park, Y. W. Park, S. Roth and M. Burghard, *Appl. Phys. Lett.*, 2000, **76**, 1875-1877.

[37] R. S. Chen, W.-C. Wang, C.-H. Chan, H.-P. Hsu, L.-C. Tien and Y.-J. Chen, *Nanoscale Res. Lett.*, 2013, **8**, 443-450.

[38] J. Lu, M. Hu, Y. Tian, C. Guo, C. Wang, S. Guo and Q. Li, *Opt. Express*, 2012, **20**, 6974-6979.

[39] B. Yan, L. Liao, Y. You, X. Xu, Z. Zheng, Z. Shen, J. Ma, L. Jong and T. Yu, *Adv. Mater.*, 2009, **21**, 2436–2440.

[40] M. R. Parida, C. Vijayan, C. S. Rout, C. S. S. Sandeep, R. Philip and P. C. Deshmukh, *J. Phys. Chem. C,* 2011,**115,** 112–117.

[41] E. Das, H. Eckert, H. Hu, I. E. Wachs, J. F. Walzer and F. J. Feher, *J. Phys. Chem.*, 1993, **97**, 8240–8243.

[42] R. Baddour-Hadjean, J. P. Pereira-Ramos, C. Navone and M. Smirnov, *Chem. Mater.*, 2008, **20**, 1916–1923.

[43] X. Miao, S. Tongay, M. K. Petterson, K. Berke, A. G. Rinzler, B. R. Appleton and A. F. Hebard, *Nano Lett.*, 2012, **12**, 2745–2750.

[44] U. Bach, D. Lupo, P. Comte, J. E. Moser, F. Weissörtel, J. Salbeck, H. Spreitzer and M. Grätzel, *Nature*, 1998, **395**, 583–585.

[45] J. Hu and R. G. Gordon, *Sol. Cells*, 1991, **30**, 437–450.

[46] S.-Y. Tai, C.-J. Liu, S.-W. Chou, F. S.-S. Chien, J.-Y. Lin and T.-W. Lin, *J. Mater. Chem.*, 2012,**22**, 24753–24759.

[47] S. Chen, J. Zhu, X. Wu, Q. Han and X. Wang, *ACS Nano*, 2010, **4**, 2822–2830.

[48] L. Cao, S. Yang, W. Gao, Z. Liu, Y. Gong, L. Ma, G. Shi, S. Lei, Y. Zhang, S. Zhang, R. Vajtai and P. M. Ajayan, *Small*, 2013, **9**, 2905–2910.

[49] S. Yoon, E. Kang, J. K. Kim, C. W. Lee and J. Lee, *Chem. Commun. (Camb).*, 2011, **47**, 1021–1023.

[50] C. Liu, Z. Yu, D. Neff, A. Zhamu and B. Z. Jang, *Nano Lett.*, 2010, **10**, 4863–4868.

[51] K. Maeda and K. Domen, *Chem. Mater.*, 2010, **22**, 612–623.

[52] Z. Chen, D. Cummins, B. N. Reinecke, E. Clark, M. K. Sunkara and T. F. Jaramillo, *Nano Lett.*, 2011, **11**, 4168–4175.

[53] J. Livage, *Materials (Basel).*, 2010, **3**, 4175–4195.

[54] J. Liu, X. Wang, Q. Peng and Y. Li, *Adv. Mater.*, 2005, **17**, 764–767.

[55] D. Yu, C. Chen, S. Xie, Y. Liu, K. Park, X. Zhou, Q. Zhang, J. Li and G. Cao, *Energy Environ. Sci.*, 2011, **4**, 858-861.

[56] L. Mai, L. Xu, C. Han, X. Xu, Y. Luo, S. Zhao and Y. Zhao, *Nano Lett.*, 2010, **10**, 4750–4755.

[57] H. Y. Yu, B. H. Kang, U. H. Pi, C. W. Park, S. Y. Choi and G. T. Kim, *Appl. Phys. Lett.*, 2005, **86**, 253102–253104.

[58] D. J. Late, *ACS Appl. Mater. Interfaces*, 2015, **7**, 5857–5862.

[59] (a) C. S. Rout, P. D. Joshi, R. V. Kashid, D. S. Joag, M. A. More, A. J. Simbeck, M. Washington, S. K. Nayak, D. J. Late, Sci. Rep. 2013, **3**, 3282. (b) R.V. Kashid, D.J. Late, S.S. Chou, Y.K. Huang, M. De, D.S. Joag, M.A. More, V. P. Dravid, Small 2013, **9**, 2730–2734 (c) S. R. Suryawanshi, P. S. Kolhe, C. S. Rout, D. J. Late and M. A. More, *Ultramicroscopy*, 2015, **149**, 51–57.

[60] K. Dewangan, N. N. Sinha, P. G. Chavan, P. K. Sharma, A. C. Pandey, M. A. More, D. S. Joag, N. Munichandraiah and N. S. Gajbhiye, *Nanoscale*, 2012, **4**, 645-651.

[61] T. Zhai, H. Liu, H. Li, X. Fang, M. Liao, L. Li, H. Zhou, Y. Koide, Y. Bando and D. Golberg, *Adv. Mater.*, 2010, **22**, 2547–2552.

[62] C. Zhou, L. Mai, Y. Liu, Y. Qi, Y. Dai and W. Chen, *J. Phys. Chem. C*, 2007, **111**, 8202–8205.

[63] R. G. Forbes, *Elev. Int. Vac. Microelectron. Conf. IVMC'[illegible] (Cat. No.98TH8382)*, 1998, 534.

[64] M. B. Shreedhara, K. Vasu, C. N. R. Rao, Zeitschrift für anorganische und allgemeine Chemie, 2014, **640**, 2737.

[65] Z. Zhang, C. Hu, Y. Xiong, R. Yang and Z. L. Wang, *Nanotechnology*, 2007, **18**, 465504-465508.

Figure 1:

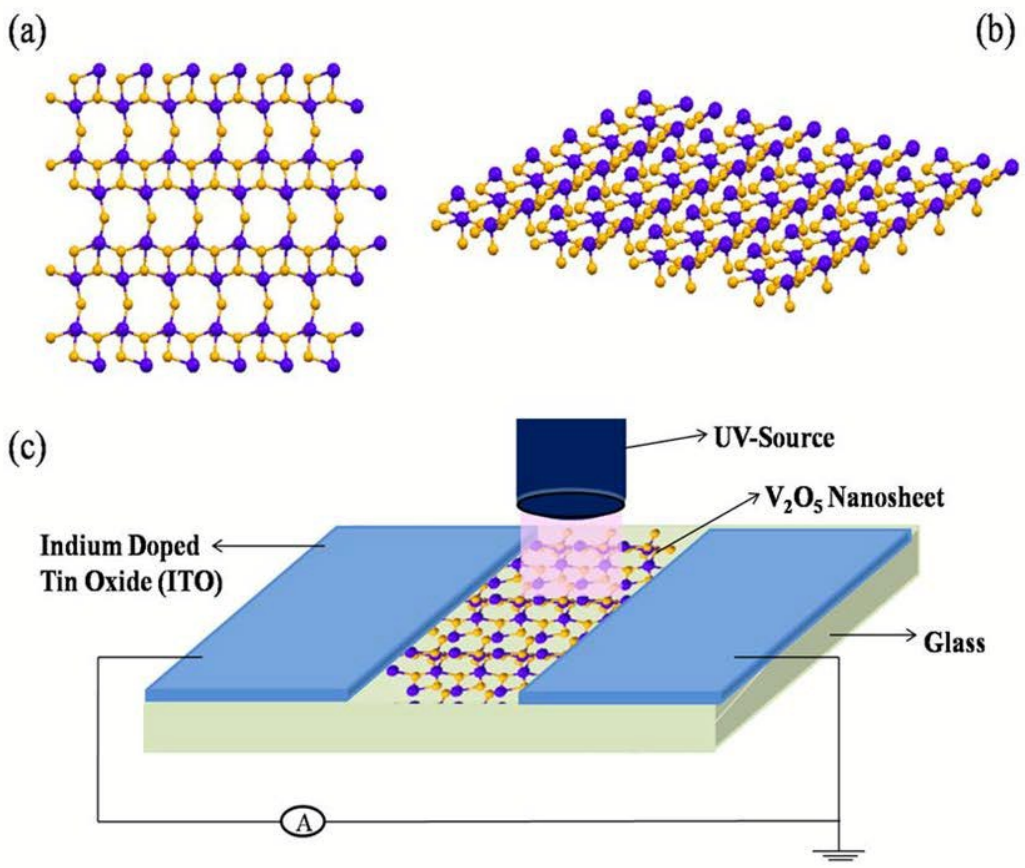

Figure 1: schematics for V_2O_5 nanosheets (a) Side view, (b) Top view and (c) Photo detection experimental set up.

Figure 2:

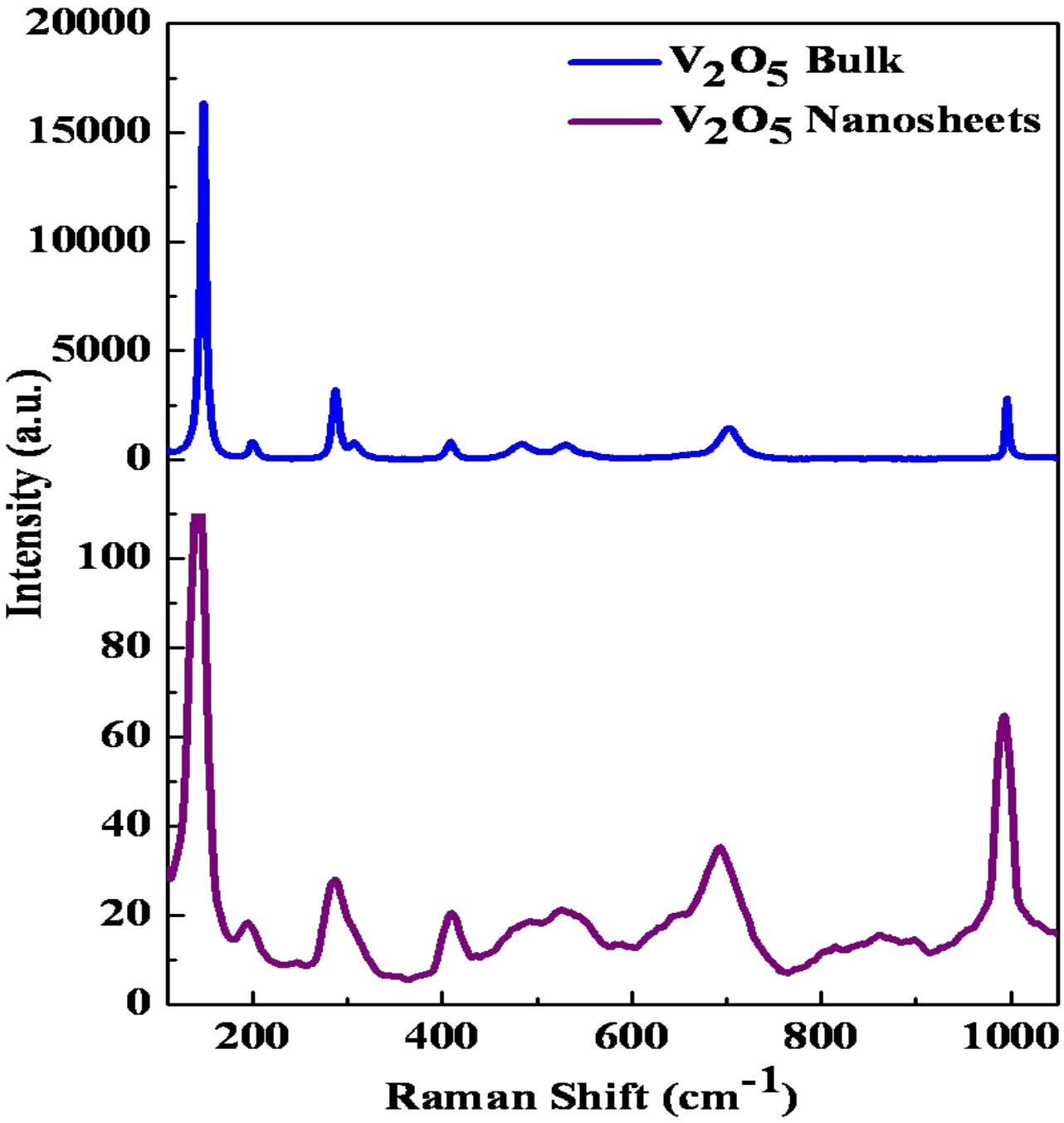

Figure 2: Raman spectrum for as obtained V_2O_5 nanosheets and V_2O_5 bulk powder.

Figure 3

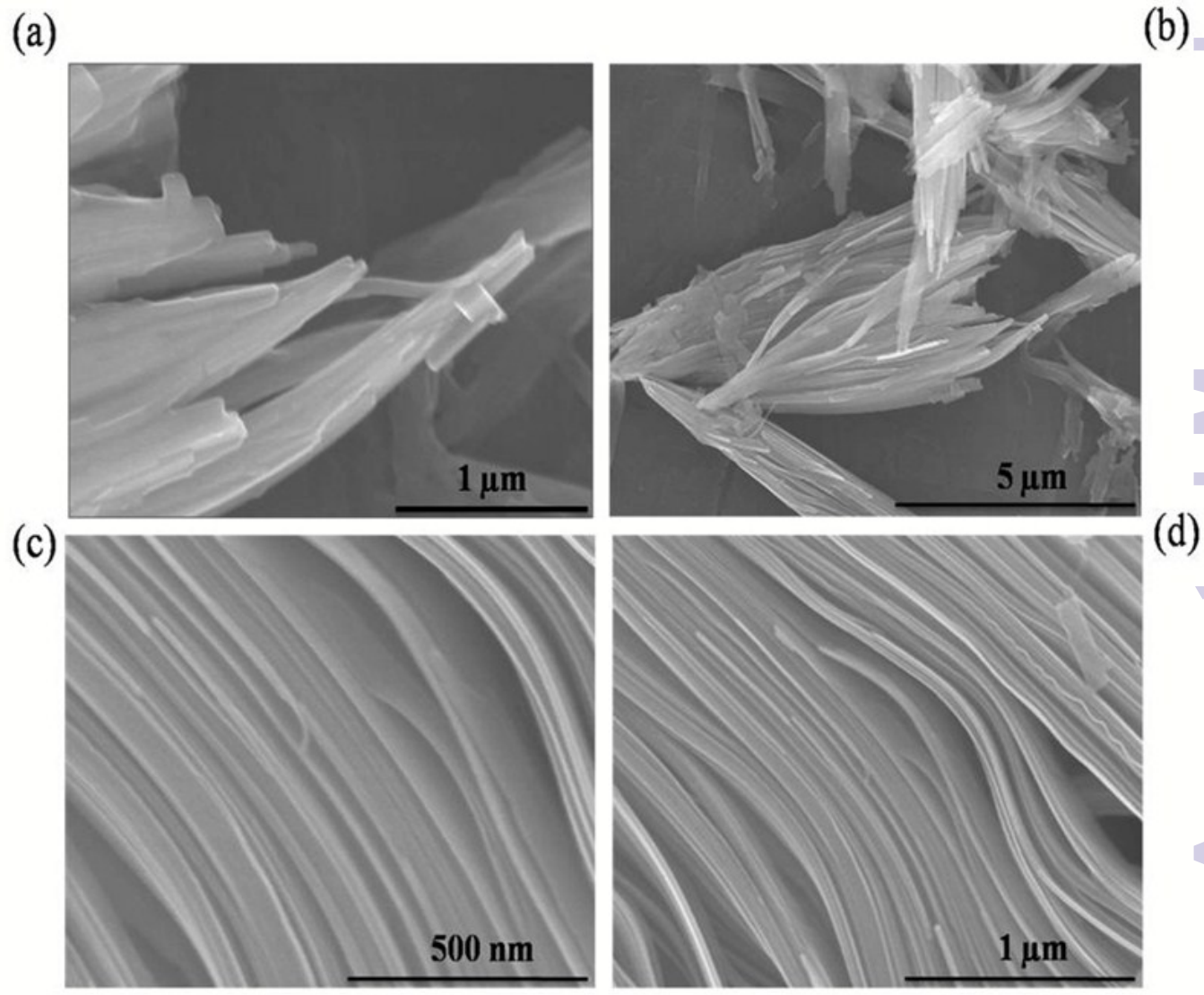

Figure 3: (a-d) FESEM images of as synthesized V_2O_5 nanosheets by using hydrothermal method.

Figure 4:

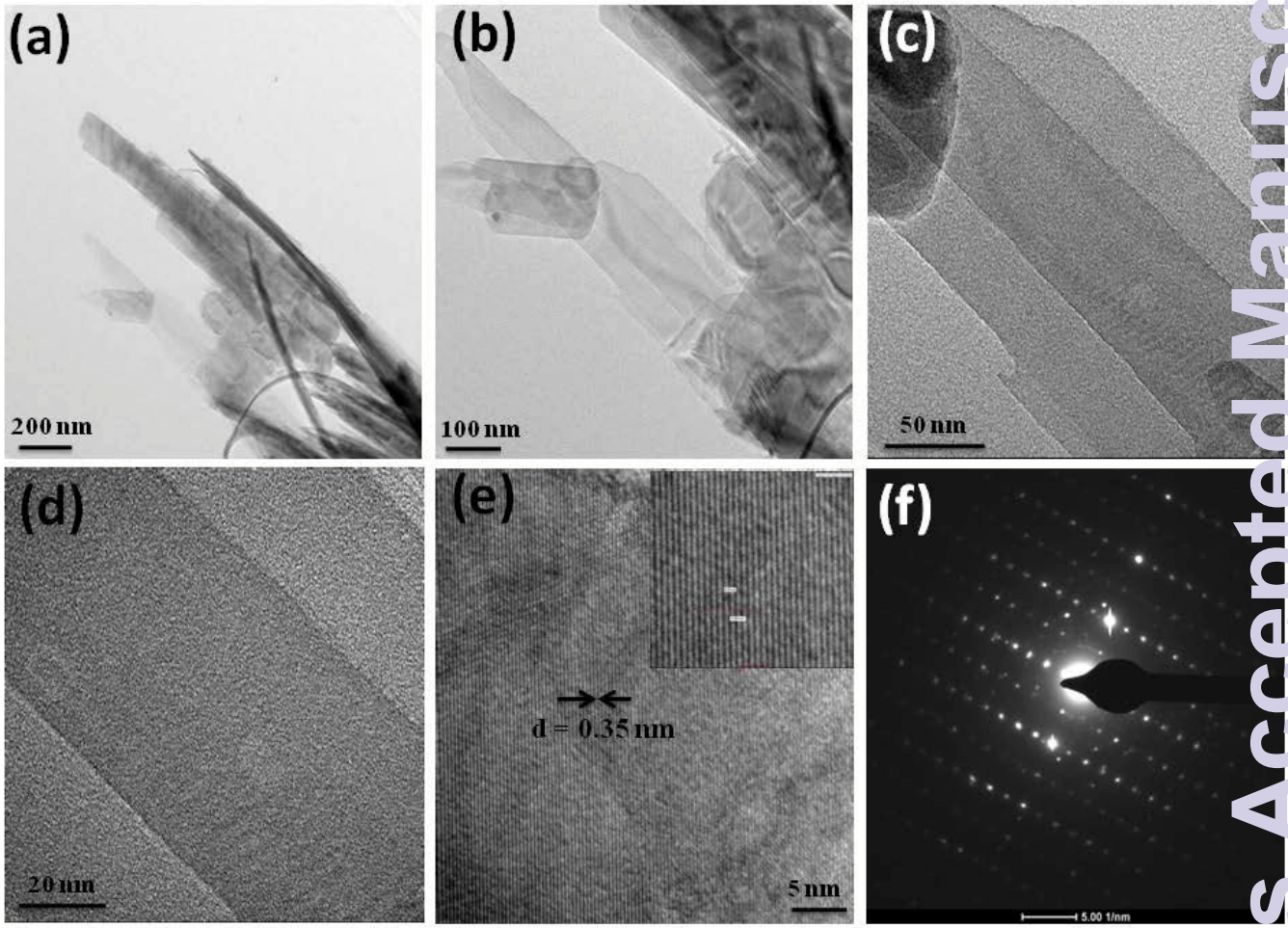

Figure 4: Typical low magnification TEM images (a) 200 nm, (b) 100 nm, (c) 50 nm, (d) 20 nm and high resolution TEM (HRTEM) image (e) 5 nm. Figure 4(f) shows the corresponding selected area electron diffraction pattern showing crystalline nature of as synthesized V_2O_5 nanosheets.

Figure 5

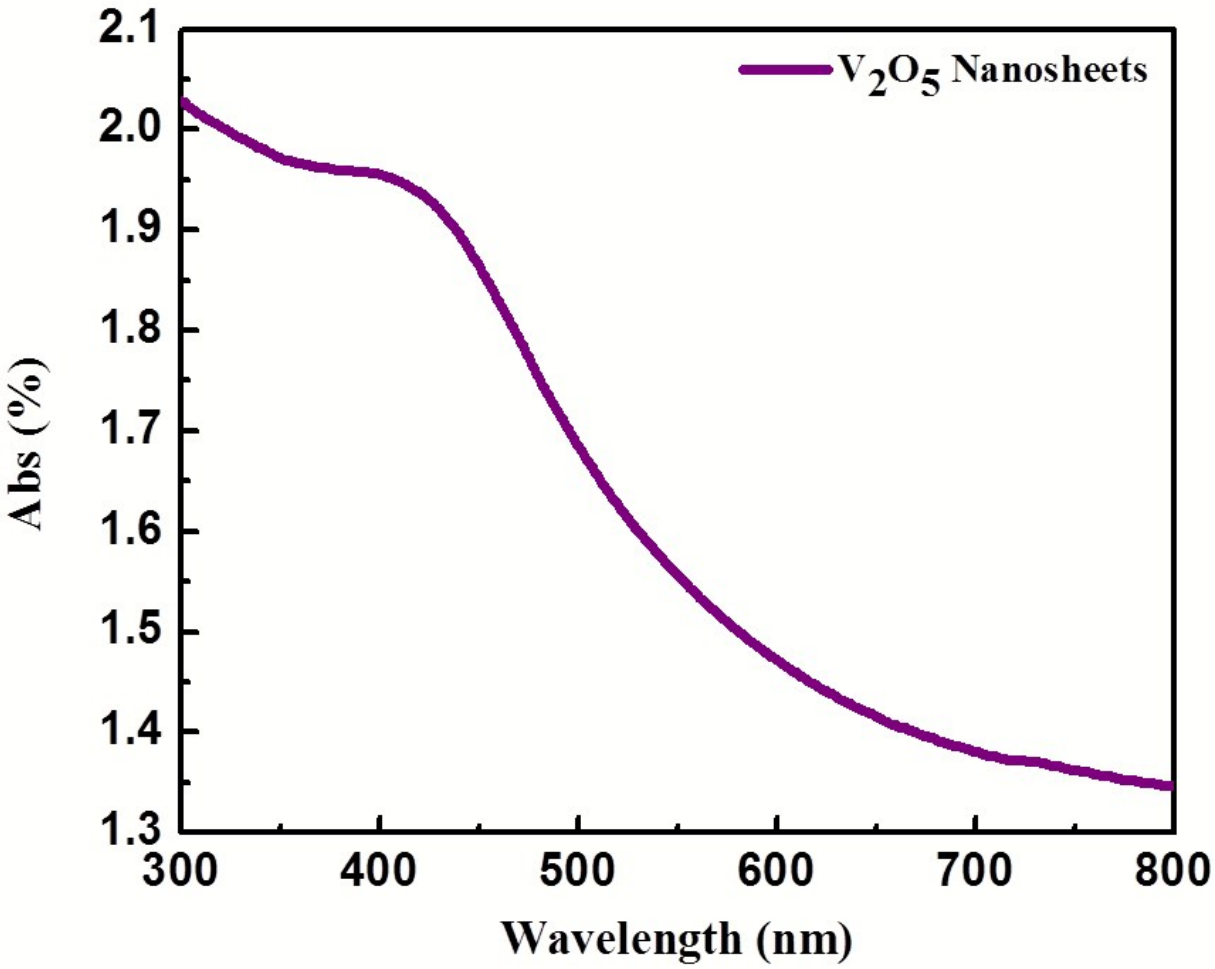

Figure 5: UV-Vis spectra of V_2O_5 nanosheets.

Figure 6:

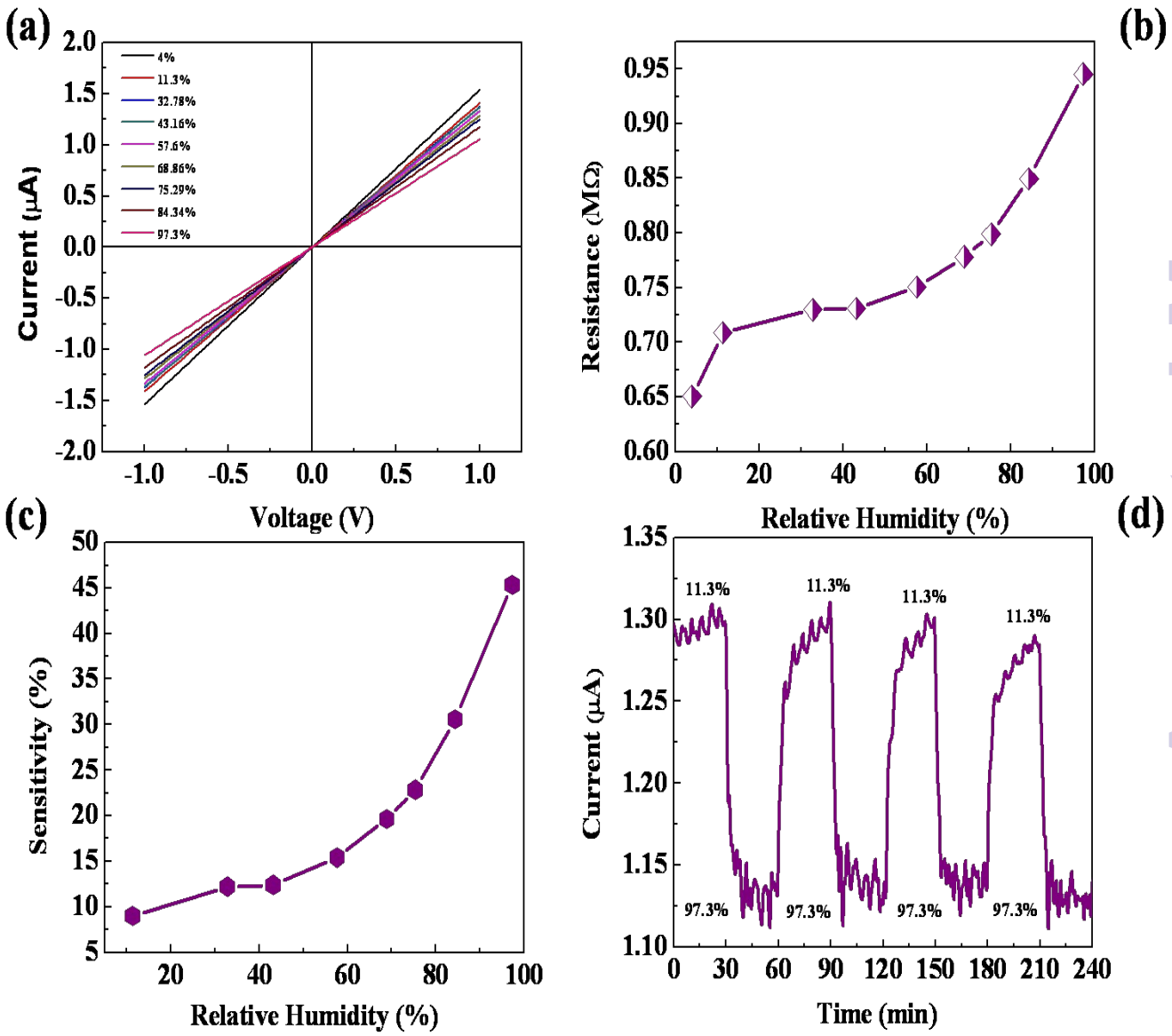

Figure 6: (a) Current-Voltage (I-V) characteristics, (b) Resistance Vs Relative Humidity, (c) Sensitivity Vs Relative Humidity and (d) Current Vs time for as obtained V_2O_5 nanosheets based sensor device.

Figure 7:

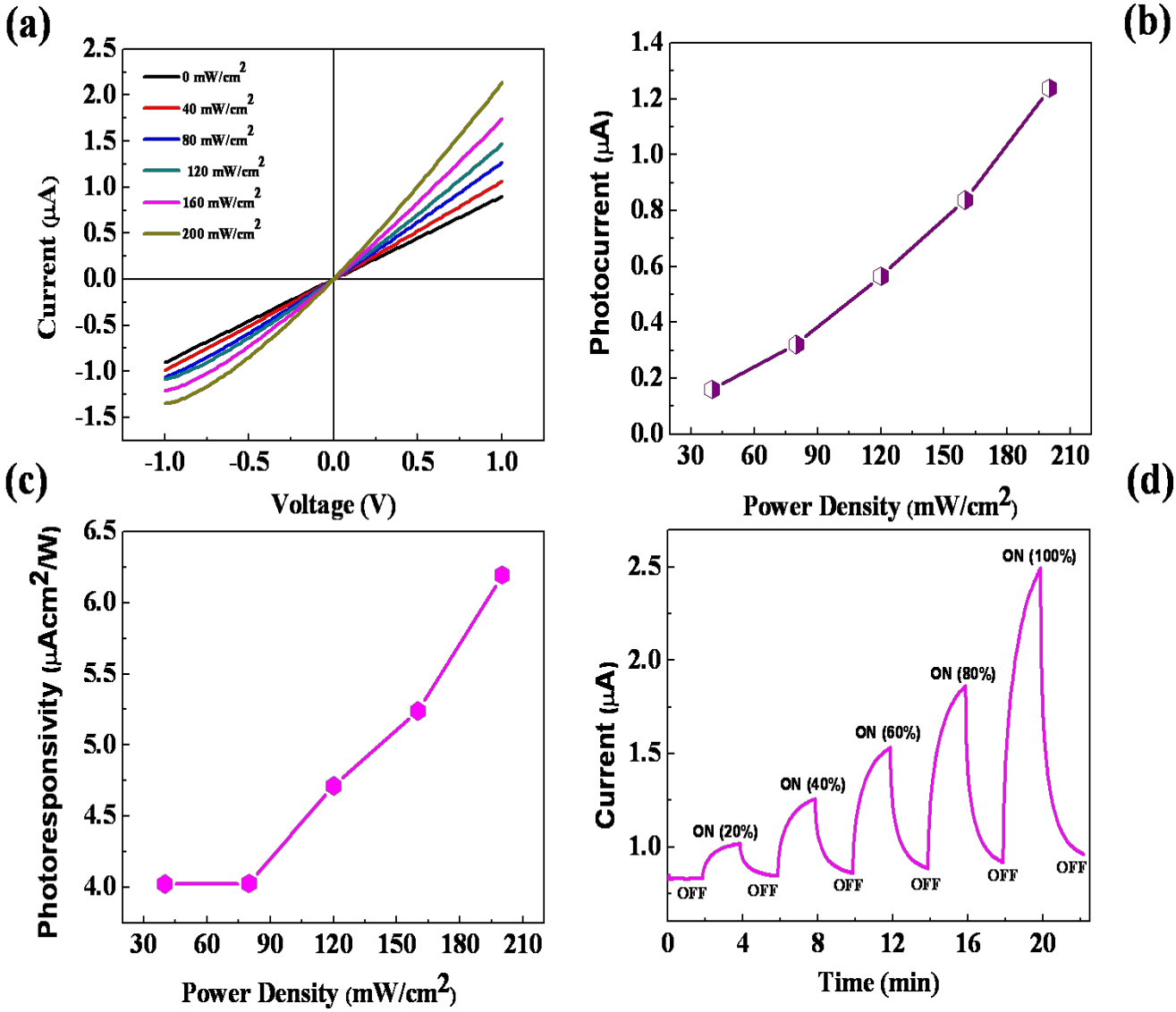

Figure 7: (a) Current-Voltage (I-V) characteristics, (b) Photocurrent Vs Power Density, (c) Photo responsivity Vs Power Density and (d) Current Vs time under the illumination of light from 0 mW/cm^2 to 200 mW/cm^2.

Figure 8:

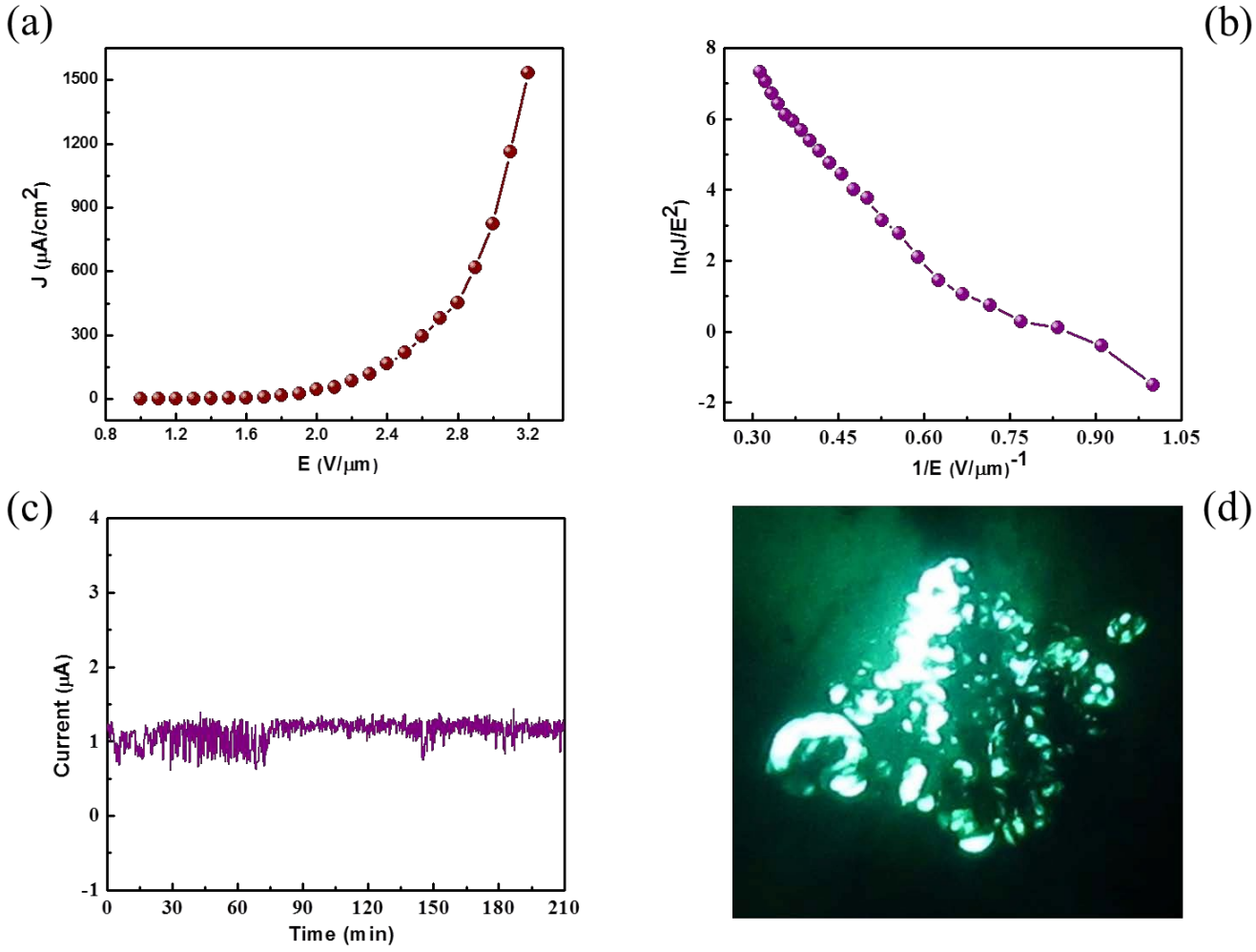

Figure 8: Field emission properties of V_2O_5 nanosheets, (a) Emission current Density Vs applied electric field (J-E plot), (b) Fowler-Nordheim plot showing nonlinear behavior indicating field electron emission from semiconducting material, (c) Field emission long term current stability (I-t plot), (d) Field emission pattern recorded at current density of 50 μA/cm^2.

Table 1

Sr. No.	Morphology	Turn-on Field (at 10μA/cm^2)	Max. Current density at applied field	References
1	Nanofiber-Bundles	~ 1.84 V/μm	213 μA/cm^2 at 3.3 V/μm	60
2	Centimeter long nanowires	~ 2.82 V/μm	14 mA/cm^2 at 4.42 V/μm	61
3	Vertically aligned nanowires	~ 8.30 V/μm	1.8 mA/cm^2 at 18 V/μm	29
4	Nanotubes array	~ 6.35 V/μm	2.1 mA/cm^2 at 9.20 V/μm	62
5	Nanorod array	~ 6.3 V/μm	2.31 mA/cm^2 at 10 V/μm	30
6	Nanosheets	~ 1.72 V/μm	1.53 mA/cm^2 at 3.2 V/μm	Present

Table 1: Comparison of field emission properties of various nanomaterials.